Highly Efficient and Bendable Organic Solar Cells with Solution-Processed Silver Nanowire Electrodes

Myungkwan Song, Dae Sung You, Kyounga Lim, Sujin Park, Sunghoon Jung, Chang Su Kim, Dong-Ho Kim, Do-Geun Kim, Jongk-Kuk Kim, Juyun Park, Yong-Cheol Kang, Jinhee Heo, Sung-Ho Jin, Jong Hyun Park, and Jae-Wook Kang**

Highly efficient and bendable organic solar cells (OSCs) are fabricated using solution-processed silver nanowire (Ag NW) electrodes. The Ag NW films were highly transparent (diffusive transmittance ≈ 95% at a wavelength of 550 nm), highly conductive (sheet resistance ≈ 10 Ω sq^{-1}), and highly flexible (change in resistance ≈ 1.1 ± 1% at a bending radius of ≈200 μm). Power conversion efficiencies of ≈5.80 and 5.02% were obtained for devices fabricated on Ag NWs/glass and Ag NWs/poly(ethylene terephthalate) (PET), respectively. Moreover, the bendable devices fabricated using the Ag NWs/PET films decrease slightly in their efficiency (to ≈96% of the initial value) even after the devices had been bent 1000 times with a radius of ≈1.5 mm.

1. Introduction

Organic solar cells (OSCs) have been actively investigated for the past decade because they have a number of advantages associated with them. They are cheap and simple to fabricate, are flexible enough to be produced by roll-to-roll manufacturing processes, and large-area versions of them can be made on flexible substrates.[1–10] Indium tin oxide (ITO), which is the preferred material for transparent conductive electrodes (TCEs), is not suitable for electrodes for flexible organic devices because it is brittle and cracks easily under mechanical stress. Moreover, owing to the rapid depletion of elemental indium and the costs associated with the various vacuum-based techniques used to produce ITO, its continued use is proving to be expensive. This, in turn, is significantly hindering the realization of low-cost and easy-to-fabricate organic optoelectronic devices. To remedy this situation, TCEs based on other materials such as carbon nanotubes (CNTs),[11–13] graphene,[14–16] and conducting polymers[17] have attracted a lot of attention and are being used to produce low-cost and highly flexible OSCs.[12,13,16] However, these TCEs typically exhibit high sheet resistances or high surface roughnesses, and this results in a reduction in the fill factor (FF) and power conversion efficiency (PCE) of the OSCs. More recently, some research groups have used nanowires (NWs) of metals such as silver,[18–26] gold,[27] and copper[28] to fabricate TCEs that show performances comparable to those of commercial ITO electrodes. For instance, Lee et al. reported the fabrication of an Ag NW mesh electrode. However, this electrode needed to be coated with a surfactant (polyvinylpyrrolidone) and had to be annealed at a high temperature (200 °C) in order to obtain good uniformity and low resistance.[22] However, it may be difficult to fabricate such Ag NW electrodes on a flexible substrate such as polyethylene terephthalate (PET). De et al. have investigated a transfer method that can be used to transfer Ag NW films onto PET substrates. However, adhesion between the PET substrates and the Ag NW films transferred using this method is poor since this method inherently involves the chemical modification of the substrate, which requires precise and special transfer techniques.[19] OSCs have been fabricated using Ag NW films formed on glass and a PET substrate, and these devices have exhibited PCEs of up to ≈4.2% and ≈3.8%, respectively.[21] Recently, Chen et al. have fabricated visibly transparent OSCs with a PCE of ≈4% by using a Ag NW film as the top electrode.[29] In order to find widespread use, OSCs that make use of Ag NW films should be cost effective

Dr. M. Song, D. S. You, K. Lim, S. Park, S. Jung, Dr. C. S. Kim, Dr. D.-H. Kim, Dr. D.-G. Kim, Dr. J.-K. Kim
Surface Technology Division
Korea Institute of Materials Science
Changwon 641-831, Republic of Korea

Prof. J.-W. Kang
Professional Graduate School of Flexible and Printable Electronics
Department of Flexible and Printable Electronics
Chonbuk National University
Jeonju 561-756, Republic of Korea
E-mail: jwkang@jbnu.ac.kr

J. Park, Prof. Y.-C. Kang
Department of Chemistry
Pukyong National University
Busan 608-737, Republic of Korea

Dr. J. Heo
Advanced Characterization and Analysis Department
Korea Institute of Materials Science
Changwon 641-831, Republic of Korea

Prof. S.-H. Jin
Department of Chemistry Education and Interdisciplinary
Program of Advanced Information and Display Materials
Pusan National University
Busan 609-735, Republic of Korea

Dr. J. H. Park
Material R&D Department
LG Display Co., Ltd. Gyeonggi-do 413-811, Republic of Korea
E-mail: jhparkjh@lgdisplay.com

DOI: 10.1002/adfm.201202646

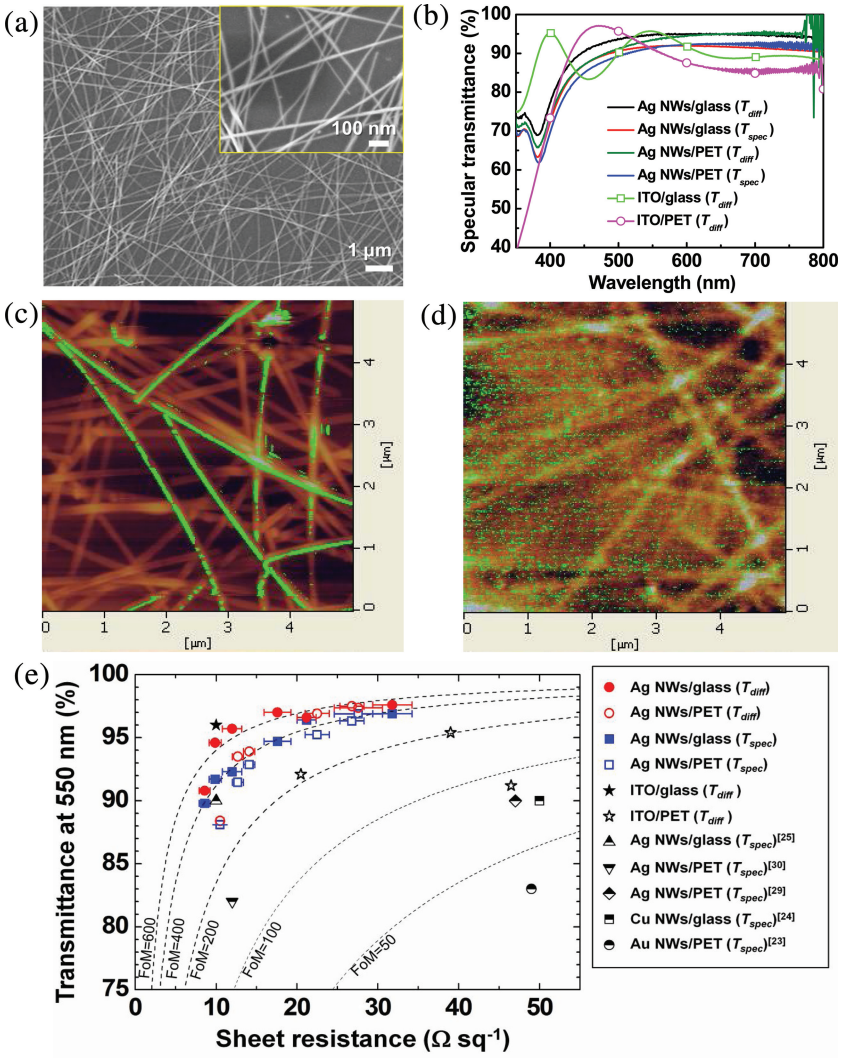

Figure 1. a) SEM image of an Ag NW electrode with R_{sheet} ≈ 10 Ω sq^{-1}. b) Specular transmittances (T_{spec}) and diffusive transmittances (T_{diff}) of Ag NW films coated onto glass and PET substrates at spin speeds of 800 rpm. For comparison, the transmittances of ITO/glass and ITO/PET are also shown. Topography images (brown color) overlapped with current images (green color) of C-AFM for c) Ag NW and d) PEDOT:PSS/Ag NW films. (e) Transmittances (at a wavelength of 550 nm) versus sheet resistances of the Ag NW electrodes. The previously reported values of ITO, Au NW, and Cu NW electrodes are also shown for comparison.

and easy to manufacture. Recently, Emmott et al. calculated the energy payback time (EPBT) and the cost of OSC modules by replacing ITO with an alternate TCE. Ag NWs prove to be excellent alternatives to ITO as the modules costs per Watt and EPBT for Ag-NW-based modules are less by almost 17% than those for ITO-based modules.[30] However, Ag NW electrodes have a number of potential issues—the performance of the films may deteriorate because of their surface roughness, and the adhesion of the films with the substrate may not be proper. Here, we report the fabrication of highly efficient and bendable OSCs using solution-processed Ag NW electrodes that were fabricated using a blend of poly (3-hexylthiophene) (P3HT)/[6,6]-phenyl-C_{61}-butyric acid methyl ester ($PC_{61}BM$), poly[4,8-bis-alkyloxy-benzo[1,2-*b*:4,5-*b*′]dithiophene-2,6-diyl-alt-4-(alkyl-1-one)thieno[3,4-b]thiophene-2,6-diyl] (PBDTTT-C)/$PC_{61}BM$, (PBDTTT-C)/[6,6]-phenyl-C_{71}-butyric acid ester ($PC_{71}BM$), and Poly[4,8-bis[(2-ethylhexyl)oxy]benzo[1,2-b:4,5-b′]dithiophene-2,6-diyl][3-fluoro-2-[(2-ethylhexyl)carbonyl] thieno[3,4-b] thiophenediyl] (PTB7-F20)/($PC_{71}BM$). These solution-processed Ag NW electrodes exhibited a low sheet resistance (R_{sheet}), which was ≈10 Ω sq^{-1}, and high transmittance, which was ≈95% at a wavelength of 550 nm (T_{550nm}). In addition, the PCE of the OSCs that used these Ag NW electrodes, which were fabricated on a glass substrate, was found to be ≈90% of that of devices with ITO electrodes (the PCEs of the OSCs using the Ag NW electrodes and those using ITO electrodes were ≈5.80% and ≈6.67%, respectively). Moreover, the flexible OSCs made using the Ag NW electrodes coated on PET substrate had a PCE of ≈5.02% with small reduction in their PCE (to ≈96% of the initial value) even after being bent 1000 times with a radius of ≈1.5 mm. This value of the PCE was much higher than that for devices that used an ITO electrode (PCE ≈ 4.48%). On the other hand, the ITO-electrode-using devices were far less flexible and exhibited a significant reduction in their PCE (to ≈63% of the initial value) after being bent. To the best of our knowledge, the efficiency and flexibility exhibited by the devices fabricated by us are the highest reported in the case of OSCs using solution-processed Ag NW electrodes.

2. Results and Discussion

Figure 1a shows a scanning electron microscopy (SEM) image of an Ag NW electrode, with R_{sheet} ≈ 10 Ω sq^{-1}, fabricated on a glass substrate by a spin-coating process at a spin speed of 800 rpm (see Supporting Information Figure S1 for images of Ag NW electrodes spin-coated on PET and glass substrates at different spin speeds). A high-magnification image in the inset of Figure 1(a) shows that the Ag NWs were squashed. The Ag NWs have an average diameter of approximately 25 ± 5 nm and an average length of a few tens of micrometers. The optical and electrical properties of the various Ag NW electrodes fabricated using different spin speeds are summarized in **Table 1**. We determined the diffusive (T_{diff}) and specular (T_{spec}) transmittance spectra of Ag NW electrodes coated on glass and PET substrates over the visible light region (Supporting Information Figure S2). When evaluating transparent Ag NW electrodes for solar cell applications, the diffusive transmittance, T_{diff}, is a more important parameter than the specular transmittance, T_{spec}. For all the electrodes tested, T_{diff} was greater than T_{spec}, and this result was in accordance with those reported previously.[28] For example, as shown in Figure 1b, the difference between the T_{diff} and T_{spec} values of the Ag

Table 1. Summary of the key parameters of the various Ag NW electrodes fabricated at different spin speeds.

Substrate	Spin-speed [rpm]	Thickness [nm]	Sheet resistance [Ω sq^{-1}]	Specular transmittance [%, at 550 nm]	Diffusive transmittance [%, at 550 nm]
Glass	600	83.2 ± 4.6	8.6 ± 0.6	90.5	90.7
Glass	800	69.6 ± 0.6	9.9 ± 0.7	91.7	94.6
Glass	1000	57.8 ± 1.1	12.0 ± 0.4	92.5	95.7
Glass	2000	40.3 ± 1.5	17.6 ± 1.6	95.7	96.5
Glass	3000	34.0 ± 1.1	23.1 ± 3.8	96.3	97.0
Glass	5000	23.7 ± 6.7	31.8 ± 2.4	97.2	98.0
PET	600	81.7 ± 3.2	10.5 ± 0.7	88.1	88.4
PET	800	66.3 ± 2.1	12.7 ± 1.6	91.4	93.5
PET	1000	56.3 ± 2.6	14.1 ± 1.0	92.8	93.9
PET	2000	38.7 ± 2.1	22.5 ± 0.6	95.2	96.9
PET	3000	31.8 ± 1.8	26.8 ± 3.6	96.3	97.3
PET	5000	21.2 ± 4.2	27.6 ± 2.7	96.8	97.5

NW electrodes on glass was about 3% for $R_{sheet} \approx 10\ \Omega\ sq^{-1}$, leading to $T_{diff,\ 550\ nm} \approx 94.6\%$, which was comparable to that of commercially available ITO electrodes on glass ($R_{sheet} \approx 10\ \Omega\ sq^{-1}$; $T_{diff,\ 550\ nm} \approx 96\%$). Furthermore, a flexible film of Ag NWs on a PET substrate exhibited $T_{diff,\ 550\ nm} \approx 93.5\%$ at $R_{sheet} \approx 13\ \Omega\ sq^{-1}$. This value was much higher than that for a 100 nm-thick ITO film on a PET substrate ($T_{diff,\ 550\ nm} \approx 91.2\%$ at $R_{sheet} \approx 46\ \Omega\ sq^{-1}$). These Ag NW films exhibited much better conductivity and higher transmittance than those reported in other studies.[24,31,32] It appears that the large length-width ratio helps to reduce the density of Ag NWs at certain conductivities. The longer Ag NWs (an average length of a few tens of micrometers) used in this study can provide a more sufficient electron percolation network than provided by shorter Ag NWs, resulting in an increase in the transmittance due to large inter-nanowire spacing, and a decrease in the sheet resistance due to small inter-nanowire junctions. The surfaces of the fabricated Ag NW films were rougher (root mean square (rms) roughness of ≈13 nm) than those of commercially available ITO films (rms roughness of ≈1 nm); therefore, the Ag NW electrodes have a higher possibility of electrical short circuiting. However, after being coated with a ≈45-nm-thick layer of PEDOT:PSS, the surface roughness of the Ag NW films decreased to ≈8 nm. This was because the Ag NWs were partially embedded in the PEDOT:PSS layer (Supporting Information Figures S3 and S4). In addition, this PEDOT:PSS coating reduced the R_{sheet} value of the Ag NW film from ≈12 to ≈10.8 Ω sq^{-1}; this reduction was caused by the decrease in the resistance of the junctions between the NWs.[24] The wire junctions naturally feature nanometer-scale gaps due to the presence of surface ligands on the wires.[33] As shown in Figure 1c (topography images overlapped with current images) we observed that current flowed along few Ag NW; thus, we suppose that the individual Ag NW were weakly contact throughout the junctions. However, PEDOT:PSS-coated Ag NWs showed an increase in the overall conductivity of the film (Figure 1d).

Figure 1e shows a plot the R_{sheet} values of the Ag NW electrodes versus their $T_{550\ nm}$ values and compares them with those previously reported for ITO, Au NW, and Cu NW electrodes. In general, the transmittance of a transparent nanostructured metallic thin film is calculated using the following relationship:[34]

$$T(\lambda) = \left(1 + \frac{188.5}{R_{sheet}} \frac{\sigma_{Op}(\lambda)}{\sigma_{DC}}\right)^{-2} \quad (1)$$

where $\sigma_{Op}(\lambda)$ is the optical conductivity and σ_{DC} is the direct current (DC) conductivity of the film. Here, the ratio σ_{DC}/σ_{Op} can be regarded a figure of merit (FoM), with its high values resulting in the TCE exhibiting desirable properties.[28,31] This expression has been fitted to the curve shown in Figure 1e and provides a resonable fit for σ_{DC}/σ_{Op} in the range of 400–600. A value of $\sigma_{DC}/\sigma_{Op} \approx 600$, such as in the case of the Ag NW film on glass when considering the diffusive transmittance, T_{diff}, is extremely large for transparent nanostructured metallic thin films. Moreover, the Ag NW film on a PET substrate exhibited $\sigma_{DC}/\sigma_{Op} \approx 400$. This value of the FoM was greater than that for the ITO film on a PET substrate ($\sigma_{DC}/\sigma_{Op} \approx 200$). We would like to point out that these values of the ratio σ_{DC}/σ_{Op}, shown in Figure 1e, are much higher than those recently reported for Ag NW,[24,31,32] Cu NW,[28] and Au NW[27] films.

In order to further investigate the use of a solution-processed Ag NW electrode as the anode in OSCs, we fabricated OSCs using the various photoactive materials; P3HT, PBDTTT-C, and PTB7-F20 as electron donors, and $PC_{61}BM$ and $PC_{71}BM$ as electron acceptors. In a typical Ag NW-based OSC, shown in **Figure 2**a, the device structure was substrate (glass or PET)/Ag NW film/poly(3,4-ethylenedioxythiophene) poly(styrenesulfonate) (PEDOT:PSS)/photoactive layer/LiF/Al. For comparison, reference OSCs with ITO/glass and ITO/PET anodes were also fabricated under similar conditions. The current density-voltage (J–V) characteristics and incident photon to current conversion efficiency (IPCE) spectra of the Ag NW/glass film-based and ITO/glass film-based OSCs under both AM 1.5G illumination and dark conditions are shown in Figure 2b-i. In addition, the averages of the values of ten samples are listed

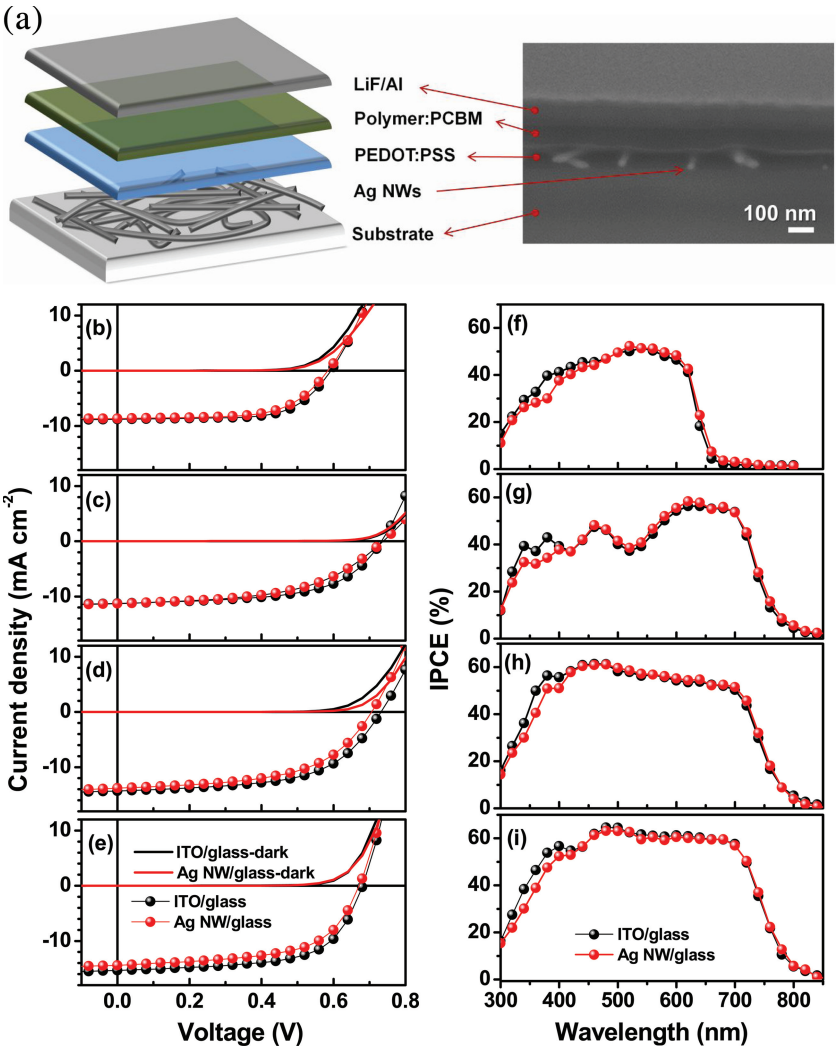

Figure 2. a) Device architecture of the OSCs based on the Ag NW electrodes, and an SEM image of the cross-section of a fabricated OSC having the following structure: glass/Ag NW film/PEDOT:PSS/PBDTTT-C:$PC_{61}BM$/LiF/Al. Characteristics *J–V* curve of Ag NWs/glass film-based and ITO/glass film-based OSCs with b) P3HT:$PC_{61}BM$, c) PBDTTT-C:$PC_{61}BM$, d) PBDTTT-C:$PC_{71}BM$, and e) PTB7-F20:$PC_{71}BM$ photoactive layers under dark conditions and AM 1.5G illumination (100 mW cm^{-2}); The IPCE spectra of the OSCs with the f) P3HT:$PC_{61}BM$, g) PBDTTT-C:$PC_{61}BM$, h) PBDTTT-C:$PC_{71}BM$, and i) PTB7-F20:$PC_{71}BM$ layers. 1,8-diiodooctane was added in a 3% volume ratio to the PBDTTT-C:$PC_{71}BM$ and PTB7-F20:$PC_{71}BM$ layers.

in **Table 2**. In general, all the Ag NW film-based OSCs exhibited performances slightly lower than those of the ITO-film-based devices. For example, as can be seen from Figure 2b, an ITO film-based OSC with a P3HT:$PC_{61}BM$ photoactive layer exhibited a short-circuit current density (J_{sc}) of ≈8.81 mA cm^{-2}, an open-circuit voltage (V_{oc}) of ≈0.59 V, and a fill factor (*FF*) of ≈65.3%, resulting in a PCE of 3.26 ± 0.14%. On the other hand, the Ag NW film-based OSC had a reasonably high PCE, which was 3.10 ± 0.16% (J_{sc} ≈ 8.65 mA cm^{-2}, V_{oc} ≈ 0.58 V, *FF* ≈ 62.5%). The Ag NW electrode-based OSCs with the layers of PBDTTT-C:$PC_{61}BM$, PBDTTT-C:$PC_{71}BM$, and PTB7-F20:$PC_{71}BM$ photoactive materials had PCEs of 4.41 ± 0.16% (J_{sc} ≈ 11.30 mA cm^{-2}, *FF* ≈ 51.4%), 5.39 ± 0.18% (J_{sc} ≈ 13.80 mA cm^{-2}, *FF* ≈ 54.8%) and 5.80 ± 0.18% (J_{sc} ≈ 14.40 mA cm^{-2}, *FF* ≈ 59.8%), respectively. These values were close (≈90%) to those of the ITO film-based OSCs fabricated under similar conditions (Figures 2b-d). The reasons for the slightly lower PCE values seen in the case of all the devices based on Ag NW electrodes were the small decreases in their J_{sc} and *FF* values. One plausible reason of the decrease in the J_{sc} value of the Ag NW electrodes-based OSCs was ascribed to the decrease in their transmittance for wavelengths around 380 nm, which was due to the plasmon absorption of Ag NWs film (see Figure 1b). However, the incident photon to current efficiency (IPCE) spectra for the Ag NW electrode-based OSCs in the range 450–800 nm, where the active layer mostly absorbs, were similar to those for the ITO-electrode-based devices except in the plasmon-absorption region (Figures 2f–i). This indicates that the slightly lower transmittance of Ag NWs did not strongly affect the device efficiency. To investigate the main reason for this, we carried out ultraviolet photoelectron spectroscopy (UPS) to measure the work functions of the Ag NW and ITO electrodes, as shown in **Figure 3**. From the secondary cutoff position of the UPS spectrum, the work function of the ITO electrode was estimated to be ≈4.4 eV, whereas that of the Ag NW electrode was 4.0 eV. The lower work function of the latter would make the contact between the anode and polymer less ohmic than the contact in the ITO electrode, leading to a decrease in the device performance.

The primary advantage of OSCs based on Ag NW films on PET substrates is that they continue to operate even when subjected to mechanical bending. **Figure 4**a shows the post-bending changes in the resistances of the electrodes based on the Ag NWs/PET (R_{sheet} ≈ 13 Ω sq^{-1}, $T_{diff,\ 550\ nm}$ ≈ 93.5%) and ITO(100 nm)/PET (R_{sheet} ≈ 46 Ω sq^{-1}, $T_{diff,\ 550\ nm}$ ≈ 91.2%) films as a function of the bending radius. The bending induced compressive stresses in the films, and the values shown are the averages of five samples. The percentage change in the resistances of the flexible TCEs is expressed as $\Delta\Omega\ \Omega_0^{-1}$, where $\Delta\Omega$ is the actual change in the resistance after bending and Ω_0 is the initial resistance. The electrode based on the Ag NWs/PET film showed high mechanical flexibility, with the percentage change in its resistance being small (≈1.1 ± 1%). This was true even after it had been bent with a bending radius R ≈ 200 μm, which corresponded to a bending strain (ε) of ≈12.5%, with $\varepsilon = h_s/(2R)$, where h_s is the substrate thickness.[35] This percentage change in the resistance was much smaller that for the electrode based on the ITO/PET film ($\Delta\Omega\ \Omega_0^{-1}$ ≈ 64.6 ± 24%). Moreover, the Ag NWs/PET film showed excellent bending fatigue strength, as shown in Figure 4b, where the bending radius was fixed at ≈1.5 mm, which corresponded to ε ≈ 1.7%.

Table 2. Photovoltaic characteristics of the OSCs under AM 1.5G illumination (100 mW cm^{-2}). The values are the averages of 10 samples of each device type. The shunt resistance (R_{sh}) and series resistance (R_s) of the OSCs were estimated by fitting the dark *J–V* curves.

Device	J_{sc} [mA cm^{-2}]	V_{oc} [V]	FF [%]	R_{sh} [Ω cm^2]	R_s [Ω cm^2]	PCE [%]
P3HT-$PC_{61}BM$ (ITO/glass)	8.81	0.59	65.31	1.15×10^4	4.53	3.26 ± 0.14
(Ag NWs/glass)	8.65	0.58	62.58	0.90×10^4	5.48	3.10 ± 0.16
PBDTTT-C:$PC_{61}BM$ (ITO/glass)	11.58	0.74	56.49	1.80×10^4	6.82	4.73 ± 0.15
(Ag NWs/glass)	11.30	0.73	51.48	1.26×10^4	9.09	4.41 ± 0.16
(ITO/PET)	10.51	0.75	51.69	1.00×10^4	12.25	3.95 ± 0.25
(Ag NWs/PET)	10.32	0.74	55.85	1.35×10^4	8.67	4.29 ± 0.12
PBDTTT-C:$PC_{71}BM$+DIO (ITO/glass)	14.32	0.73	56.96	6.81×10^4	2.21	5.80 ± 0.17
(Ag NWs/glass)	13.80	0.71	54.87	4.97×10^4	2.67	5.39 ± 0.18
(ITO/PET)	11.43	0.71	49.63	9.31×10^3	14.66	3.92 ± 0.35
(Ag NWs/PET)	11.45	0.71	53.10	1.28×10^4	9.07	4.41 ± 0.12
PTB7-F20:$PC_{71}BM$+DIO (ITO/glass)	15.32	0.68	62.55	9.28×10^4	2.07	6.67 ± 0.30
(Ag NWs/glass)	14.40	0.67	59.81	6.17×10^4	2.44	5.80 ± 0.18
(ITO/PET)	13.03	0.67	52.92	1.58×10^4	7.82	4.48 ± 0.58
(Ag NWs/PET)	13.10	0.67	56.89	3.95×10^4	5.58	5.02 ± 0.13

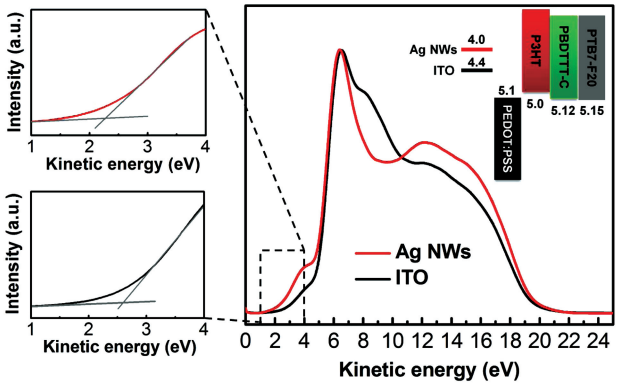

Figure 3. UPS spectra for Ag NW and ITO films. From the secondary cutoff positions, the work function of the samples can be estimated. Schematic description of the electronic structure of transparent electrodes based on UPS spectra and polymer layers from the literature.[36,37]

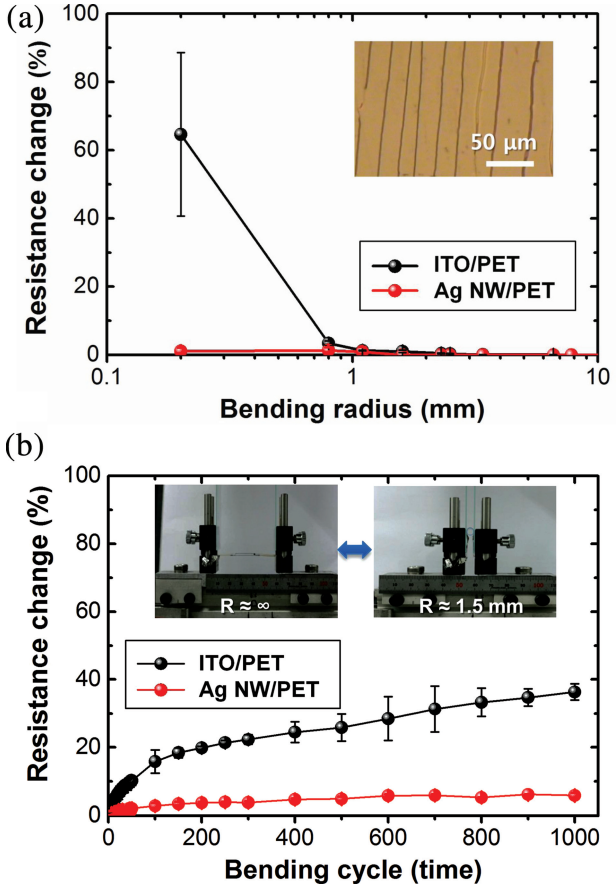

Figure 4. (a) Measured changes in the resistances of the electrodes based on the flexible Ag NW/PET and ITO(100 nm)/PET films a function of the bending radius. Inset figure: optical image of the electrode based on the ITO/PET film after being bent with a radius of ≈0.8 mm. (b) Change in resistance as a function of the number of bending cycles with the bending radius (R) ≈ 1.5 mm.

Even after being bent 1000 times, the electrode based on the Ag NWs/PET film exhibited only a slight increase in the $\Delta\Omega\ \Omega_0^{-1}$ value (≈5.9 ± 0.4%), whereas that of the electrode based on the ITO/PET film increased drastically ($\Delta\Omega\ \Omega_0^{-1} \approx 36.3 \pm 13.7\%$)

Figure 5a–f show the *J–V* characteristics and IPCE spectra of the flexible OSCs fabricated using the Ag NWs/PET and ITO/PET films. The Ag NWs/PET film-based OSCs with the PBDTTT-C/$PC_{61}BM$, PBDTTT-C/$PC_{71}BM$, and PTB7-F20/$PC_{71}BM$ photoactive layers exhibited much higher device performances than did the ITO/PET film-based device. This was due to their J_{sc} and *FF* values being higher than that of the ITO/PET film-based device. For example, the PTB7-F20/$PC_{71}BM$ device with an Ag NWs/PET electrode had a PCE of 5.02 ± 0.13% ($J_{sc} \approx 13.10$ mA cm^{-2}, $FF \approx 56.9\%$), which was much higher than that of the ITO/PET film-based device (PCE ≈ 4.48 ± 0.58%%, $J_{sc} \approx 13.03$ mA cm^{-2}, $FF \approx 52.9\%$). In case of

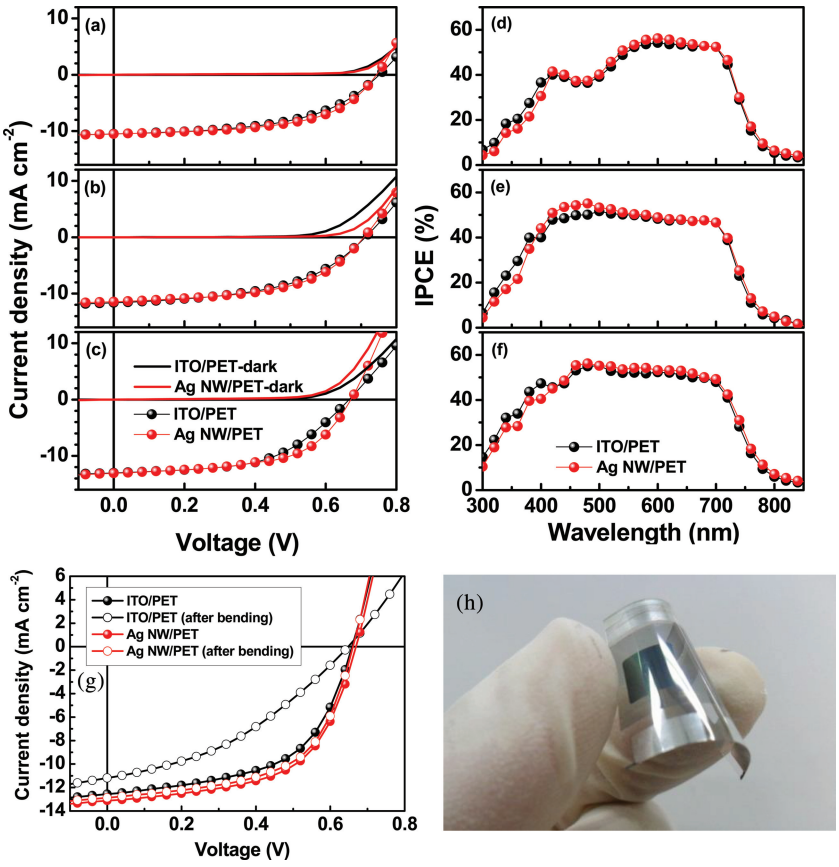

Figure 5. Characteristics *J–V* curves of the Ag NWs/PET film-based and ITO/PET film-based flexible OSCs with a) PBDTTT-C:$PC_{61}BM$, b) PBDTTT-C:$PC_{71}BM$, and c) PTB7-F20:$PC_{71}BM$ photoactive layers under dark conditions and AM 1.5G illumination (100 mW cm^{-2}); IPCE spectra of the OSCs with the d) PBDTTT-C:$PC_{61}BM$, e) PBDTTT-C:$PC_{71}BM$, and f) PTB7-F20:$PC_{71}BM$ layers. 1,8-diiodooctane was added in a 3% volume ratio to the PBDTTT-C:$PC_{71}BM$ and PTB7-F20:$PC_{71}BM$ layers. g) The *J–V* characteristics of the OSCs with the PTB7-F20-C:$PC_{71}BM$ layer after 1000 cycles of the bending test with the bending radius R ≈ 1.5 mm. h) Photograph of Ag NW/PET film-based flexible OSCs.

the ITO/PET film-based OSCs, the 100 nm-thick ITO anode cracked easily during the fabrication process, particularly during the spin-coating of the PEDOT:PSS and active layers, resulting in a lower PCE and a much larger deviation in the device efficiency (± 0.58%) than that for the Ag NWs/PET film-based devices (± 0.13%) (the average values of ten samples were considered) (see Supporting Information Figure S5 and Table 2). The Ag NWs/PET film-based OSCs exhibited an extremely high degree of flexiblity, as can be seen from Figure 5g. These devices were also highly durable, and even after being bent 1000 times with a radius $R \approx 1.5$ mm, they exhibited little change in their *J–V* characteristics. The post-bending PCE value of these devices was ≈96% of the initial value, whereas in the case of the ITO/PET film-based device, it was ≈ 63% of the initial value.

3. Conclusion

In summary, we were able to fabricate highly efficient and bendable OSCs using solution-processed Ag NW electrodes. The Ag NWs/glass film-based electrode exhibited a lower R_{sheet} value (of ≈10 Ω sq^{-1}) and higher $T_{diff,\ 550nm}$ value (of ≈95%) when compared to a ITO/glass film-based electrode (R_{sheet} ≈ 10 Ω sq^{-1}, $T_{diff,\ 550nm}$ ≈ 96%). Furthermore, the values of the mechanical flexibility ($\Delta\Omega\ \Omega_0^{-1} \approx 1.1 \pm 1\%$ at R ≈ 200 μm) and electrical/optical parameters ($T_{diff,\ 550nm}$ ≈ 93.5%, R_{sheet} ≈ 13 Ω sq^{-1}) of the flexible Ag NWs/PET film-based anode were much higher than those of the ITO/PET film-based anode ($T_{diff,\ 550nm}$ ≈ 91.2%, R_{sheet} ≈ 46 Ω sq^{-1}, $\Delta\Omega\ \Omega_0^{-1} \approx 64.6 \pm 24\%$). Overall, the PCE of the Ag NWs/glass film-based OSCs that had a layer of PTB7-F20/$PC_{71}BM$ was found to ≈90% of that of the devices based on the ITO/glass film-based electrodes, with the PCEs of the former and the latter being ≈5.80 ± 0.18% and ≈6.67 ± 0.30%, respectively. Moreover, the flexible OSCs fabricated using the Ag NWs/PET films had a PCE of ≈5.02 ± 0.13%, and this value decrease slightly in their PCE (to ≈96% of the initial value) even after the devices had been bent 1000 times with a radius of ≈1.5 mm. In addition, this value was much higher than that for the device based on the ITO/PET film (PCE ≈ 4.48 ± 0.58%), which was also less flexible and exhibited a significant reduction in its PCE (to ≈63% of the initial value) after bending. These results demonstrate that solution-processed Ag NW electrodes can be sucessfully used in flexible, large-area OSCs and solid-state lighting devices in the future.

4. Experimental Section

Preparation of the Ag NW and ITO Films: The Ag NW films were prepared using the spin-coating process and were formed on precleaned glass or PET substrates that were attached to a supporting glass substrate. An as-received dispersion containing Ag NWs (Cambrios ClearOhm Ink) was spin coated for 40 s at speeds ranging from 600–5000 rpm. The dispersion was sonicated for 300 s and shaken well before being the spin-coating process. The formed Ag NW films were annealed at ≈120 °C for 5 min in a glove box filled with nitrogen.

The ITO/PET films were vacuum sputtered in our laboratory and the ITO/glass film was obtained commercially (Shinhan SNP Co. Ltd). The ITO/PET films were formed by depositing a layer of ITO on a 50-μm-thick PET substrate (SKC Co. Ltd.) by radio-frequency (RF) superimposed DC magnetron sputtering. An ITO target comprising 10 wt% tin was used for the sputtering. The ITO sputtering was carried out using an Ar gas flow rate of 30 sccm, an O_2 gas flow rate of 0.3 sccm, and a working pressure of $\approx 1.5 \times 10^{-1}$ torr. The distance between the substrate and the plasma source was ≈100 mm. The DC power was controlled by keeping the current constant (≈0.5 A), and ≈50 W of RF power was imposed simultaneously. The growth rate of the film was ≈0.316 nm s^{-1}, and an ITO film with a final thickness of ≈100 nm was deposited.

Fabrication of the Organic Solar Cells (OSCs): The OSCs were fabricated using Ag NW film-coated glass and PET substrates with R_{sheet} values of ≈10 Ω sq^{-1} and ≈13 Ω sq^{-1}, respectively. Buffer layers of poly(3,4-ethylenedioxylenethiophene) (PEDOT-PSS) (Clevious P) diluted using isopropyl alcohol (IPA) to improve the wettability for ITO

and Ag NW electrodes, with the ratio of PEDOT-PSS:IPA being 1:2, were deposited on the substrates using a spin coater after passing through a 0.45 μm filter. The final thickness of the layers was ≈45 nm. These substrates were then baked in a glove box at 150 °C for 10 min. Mixtures of P3HT:$PC_{61}BM$ (10 mg:20 mg) and PBDTTT-C:$PC_{61}BM$ (10 mg:20 mg) were dissolved in 1,2-dichlorobenzene (1 mL). In addition, mixtures of PBDTTT-C:$PC_{71}BM$ (8 mg:12 mg) and PTB7-F20:$PC_{71}BM$ (8 mg:12 mg) were dissolved in chlorobenzene (1 mL). The P3HT used in this study was purchased from Luminescence Technology Corp.; $PC_{61}BM$ from Nano-C; $PC_{71}BM$ from Solemme BV; and PBDTTT-C and PTB7-F20 from 1-material. The mixed solutions were stirred at 50 °C for 12 h. 1,8-Diiodooctane (DIO) (Sigma Aldrich) was then added in a volume ratio of 3% to the solutions containing PBDTTT-C:$PC_{71}BM$ and PTB7-F20:$PC_{71}BM$ before the spin-coating process. The thickness of the active layer made of P3HT:$PC_{61}BM$ was ≈250 nm, whereas the thickness of those made of PBDTTT-C:$PC_{61}BM$, PBDTTT-C:$PC_{71}BM$, and PTB7-F20:$PC_{71}BM$ was ≈100 nm. Then, the substrates were subjected to vacuum-like conditions (2×10^{-6} torr), and a layer of LiF (0.7 nm), and on top of that, a layer of Al (100 nm) were deposited on them. The area of the top metal electrode, comprising the active area of the solar cells, was found to be ≈0.36 cm^2. For comparison, control OSCs with ITO/glass anodes were also fabricated under similar conditions.

Bending Test: To test for mechanical stability, a bending test system was designed in house. It was used to measure the critical radii of the Ag NWs/PET and ITO/PET films. The system consisted of the two contact points: one of the points was fixed and the other could be moved laterally. Supporting Information Figure S6 shows the procedure followed in the bending tests of flexible OSCs. The bending tests resulted in compressive stresses and were performed on unencapsulated devices in a nitrogen atmosphere.

Characterization: The transmittance spectra were measured using an ultraviolet-visible spectrophotometer (Cary 5000, Varian). Conductive atomic force microscopy (C-AFM, Seiko E-Sweep) was conducted for evaluating the surface current flow in the films. For current images of the films, contact mode and tips with Pt/Ir were chosen and a 0.1 V bias was applied to each film. UPS was performed using a gas discharge UV source housed at ESCALAB MKII (He I radiation; hν = 21.2 eV). The take-off angle was set at 45° relative to the sample surface. During UPS, the sample was biased at −3.0 V relative to the ground potential in order to observe low energy secondary electron cutoff. The UV photoelectron emission was detected with a concentric hemispherical analyzer with a pass-energy of 50 eV. The performances of the OSCs were measured under simulated AM 1.5 illumination with an irradiance of 100 mW cm^{-2} (PEC-L11, Pecell Technologies Inc.). The irradiance of the sunlight-simulating illumination was calibrated using a standard Si photodiode detector fitted with a KG5 filter. The *J–V* curves were recorded automatically using a Keithley 2400 SourceMeter source measurement unit. The quantum efficiency measurement system used to determine the IPCE spectra (Oriel IQE-200) used a 250 W quartz tungsten halogen (QTH) lamp as the light source and had a monochromator, an optical chopper, a lock-in amplifier, and a calibrated silicon photodetector. The film thicknesses, sheet resistances, and optical transmittances were measured using a surface profiler (Alpha Step P-11, Tencor Instruments), a four-point probe system (Mitsubishi Chemical Corporation), and a UV-vis spectrophotometer (Cary 5000, Varian), respectively. The scanning electron microscopy (SEM) micrographs were obtained using a JSM-6700F field emission scanning electron microscope.

Supporting Information

Supporting Information is available from the Wiley Online Library or from the author.

Acknowledgements

M.S., D.S.Y., and K.L. contributed equally to this paper. This study was supported by the New and Renewable Energy program of the Korea Institute of Energy Technology Evaluation and Planning (KETEP) (Grant no. 20113010010030 and 20103020010050) funded by the Ministry of the Knowledge Economy and by a grant from the National Research Foundation of Korea (NRF) funded by the Ministry of Education, Science and Technology (MEST) of Korea (No. 2011-0028320).

Received: September 13, 2012
Revised: December 30, 2012
Published online: April 10, 2013

[1] T. R. Andersen, T. T. L. Olsen, B. Andreasen, A. P. L. Böttiger, J. E. Carlé, M. Helgesen, E. Bundgaard, K. Norrman, J. W. Andreasen, M. Jørgensen, F. C. Krebs, *ACS Nano* **2011**, *5*, 4188.
[2] W. I. Jeong, J. Lee, S. Y. Park, J. W. Kang, J. J. Kim, *Adv. Funct. Mater.* **2011**, *21*, 343.
[3] H. Jin, C. Tao, M. Velusamy, M. Aljada, Y. Zhang, M. Hambsch, P. L. Burn, P. Meredith, *Adv. Mater.* **2012**, *24*, 2572.
[4] S. Y. Park, Y. J. Kang, S. Lee, D. G. Kim, J. K. Kim, J. H. Kim, J. W. Kang, *Sol. Energy Mater. Sol. Cells* **2011**, *95*, 852.
[5] S. H. Eom, H. Park, S. H. Mujawar, S. C. Yoon, S. S. Kim, S. I. Na, S. J. Kang, D. Khim, D. Y. Kim, S. H. Lee, *Org. Electron.* **2010**, *11*, 1516.
[6] L. Dou, J. You, J. Yang, C. C. Chen, Y. He, S. Murase, T. Moriarty, K. Emery, G. Li, Y. Yang, *Nat. Photonics* **2012**, *6*, 180.
[7] Y. Sun, G. C. Welch, W. L. Leong, C. J. Takacs, G. C. Bazan, A. J. Heeger, *Nat. Mater.* **2011**, *11*, 44.
[8] H. Zhou, L. Yang, A. C. Stuart, S. C. Price, S. Liu, W. You, *Angew. Chem.* **2011**, *123*, 3051.
[9] K. M. O'Malley, C. Z. Li, H. L. Yip, A. K. Y. Jen, *Adv. Energy Mater.* **2012**, *2*, 82.
[10] J. B. Kim, P. Kim, N. C. Pégard, Soong Ju Oh, C. R. Kagan, J. W. Fleischer, H. A. Stone, Y. L. Loo, *Nat. Photonics* **2012**, *6*, 327.
[11] Z. Yang, T. Chen, R. He, G. Guan, H. Li, L. Qiu, H. Peng, *Adv. Mater.* **2011**, *23*, 5436.
[12] T. Chen, S. Wang, Z. Yang, Q. Feng, X. Sun, L. Li, Z. S. Wang, H. Peng, *Angew. Chem. Int. Ed.* **2011**, *50*, 1815.
[13] J. H. Huang, J. H. Fang, C. C. Liu, C. W. Chu, *ACS Nano* **2011**, *5*, 6262.
[14] Z. Liu, J. Li, Z. H. Sun, G. Tai, S. P. Lau, F. Yan, *ACS Nano* **2012**, *6*, 810.
[15] K. S. Kim, Y. Zhao, H. Jang, S. Y. Lee, J. M. Kim, K. S. Kim, J. H. Ahn, P. Kim, J. Y. Choi, B. H. Hong, *Nature* **2009**, *457*, 706.
[16] J. Wu, H. A. Becerril, Z. Bao, Z. Liu, Y. Chen, P. Peumans, *Appl. Phys. Lett.* **2008**, *92*, 263302.
[17] S. I. Na, G. Wang, S. S. Kim, T. W. Kim, S. H. Oh, B. K. Yu, T. Lee, D. Y. Kim, *J. Mater. Chem.* **2009**, *19*, 9045.
[18] E. C. Garnett, W. Cai, J. J. Cha, F. Mahmood, S. T. Connor, M. G. Christoforo, Y. Cui, M. D. McGehee, M. L. Brongersma, *Nat. Mater.* **2012**, *11*, 241.
[19] S. De, T. M. Giggins, P. E. Lyons, E. M. Doherty, P. N. Nirmalraj, W. Blau, J. J. Boland, J. N. Coleman, *ACS Nano* **2009**, *3*, 1767.
[20] W. Gaynor, J. Y. Lee, P. Peumans, *ACS Nano* **2010**, *4*, 30.
[21] W. Gaynor, G. F. Burkhard, M. D. McGehee, P. Peumans, *Adv. Mater.* **2011**, *23*, 2905.
[22] J. Y. Lee, S. T. Connor, Y. Cui, P. Peumans, *Nano Lett.* **2010**, *10*, 1276.
[23] D. S. Leem, A. Edwards, M. Faist, J. Nelson, D. D. C. Bradley, J. C. de Mello, *Adv. Mater.* **2011**, *23*, 4371.
[24] L. Yang, T. Zhang, H. Zhou, S. C. Price, B. J. Wiley, W. You, *ACS Appl. Mater. Interfaces* **2011**, *3*, 4075.
[25] F. S. F. Morgenstern, D. Kabra, S. Massip, T. J. K. Brenner, P. E. Lyons, J. N. Coleman, R. H. Friend, *Appl. Phys. Lett.* **2011**, *99*, 183307.

[26] J. Ajuria, I. Ugarte, W. Cambarau, I. Etxebarria, R. Tena-Zaera, R. Pacios, *Sol. Energy Mater. Sol. Cells* **2012**, *102*, 148.
[27] P. E. Lyons, S. De, J. Elias, M. Schamel, L. Philippe, A. T. Bellew, J. J. Boland, J. N. Coleman, *J. Phys. Chem. Lett.* **2011**, *2*, 3058.
[28] H. Wu, L. Hu, M. W. Rowell, D. Kong, J. J. Cha, J. R. McDonough, J. Zhu, Y. Yang, M. D. McGehee, Y. Cui, *Nano Lett.* **2010**, *10*, 4242.
[29] C.-C. Chen, L. Dou, R. Zhu, C. -H. Chung, T. -B. Song, Y. B. Zheng, S. Hawks, G. Li, P. S. Weiss, Y. Yang, *ACS Nano* **2012**, *6*, 7185.
[30] C. J. M. Emmott, A. Urbina, J. Nelson, *Sol. Energy Mater. Sol. Cells* **2012**, *97*, 14.
[31] V. Scardaci, R. Coull, P. E. Lyons, D. Rickard, J. N. Coleman, *Small* **2011**, *7*, 2621.
[32] Z. Yu, Q. Zhang, L. Li, Q. Chen, X. Niu, J. Liu, Q. Pei, *Adv. Mater.* **2011**, *23*, 664.
[33] E. C. Garnett, W. Cai, J. J. Cha, F. Mahmood, S. T. Connor, M.G. Christoforo, Y. Cui, M. D. McGehee, M. L. Brongersma, *Nat. Mater.* **2012**, *11*, 241.
[34] M Dressel, G. Gruner, *Electrodynamics of Solids: Optical Properties of Electrons in Matter*; Cambridge University Press, Cambridge **2002**.
[35] S. I. Park, J. H. Ahn, X. Feng, S. Wang, Y. Huang, J. A. Rogers, *Adv. Funct. Mater.* **2008**, *18*, 2673.
[36] H.-Y. Chen, J. Hou, S. Zhang, Y. Liang, G. Yang, Y. Yang, L. Yu, Y. Wu, G. Li, *Nat. Photonics* **2009**, *3*, 649.
[37] H.-L. Yip, A. K.-Y. Jen, *Energy Environ. Sci.* **2012**, *5*, 5994.